Numerical Analysis of Sound Generation and Transmission from Flapping Wings

Yoshinobu Inada [a*], Masateru Maeda [b], Takashi Moriyama [b**], Hikaru Aono [c], Hao Liu [b], and Takashi Aoyama [a]

[a] Japan Aerospace Exploration Agency (JAXA), Japan
[b] Chiba University, Japan
[c] University of Michigan, USA

Abstract—Insects generate sound by their flapping wings as a consequence of spatial and temporal changes of pressures on the wing surface and vortices generated by the wing motion. To clarify the mechanism of sound generation, hybrid method combining CFD techniques and acoustic analysis is incorporated here and detailed characteristics of flapping sound, e.g. directivity of transmission or spectrum distributions, are clarified.

Index Terms— Flapping sound, Insect, CFD, Acoustic Analysis

I. INTRODUCTION

Buzzing or bumbling sound of bees or mosquitoes is extensively well-known sound generation by insects. Some species of insects also use flapping sound for a mutual communication such as a courtship song[(1)]. The analysis of sound generation of flapping wing and its control can, therefore, explain how insects control flapping sound for survival and reproduction, e.g. to avoid detection by enemies or to tune sound tone to attract opposite-sex targets, thus leading to the novel technology to realize silent flapping flyer or new type communication devices. The hybrid method combining CFD and acoustic analysis is incorporated here to provide an effective tool for clarifying the mechanism of flapping sound generation and its control principles. The NS-based CFD[(2, 3)] offers detailed vortex aspects and induced pressure distributions on the wing surfaces which act as the flapping sound sources. The acoustic analysis based on Ffowcs-Williams and Hawkings (FW-H) equation[(4, 5)] offers detailed characteristics of sound waves around the insect by using sound sources calculated in CFD. By using this hybrid method, the flapping sound of two different flight modes of hawkmoth, i.e. hovering and forward moving flights, are analyzed in this study to clarify the decisive factors to control flapping sound.

II. MATERIALS AND METHODS

A. CFD solver, calculation grid, and insect model

The governing equations in CFD calculation are the three-dimensional incompressible unsteady Navier-Stokes (NS) equations solved with the pseudo-compressibility technique. The equations are written in a strong conservative form for momentum and mass, and non-dimensionalized in an integral form, such that:

$$\int_{V(t)} (\partial \boldsymbol{q}/\partial\tau) dV + \frac{\partial}{\partial t}\int_{V(t)} \boldsymbol{Q} dV + \int_{S(t)} \left(\boldsymbol{f} - \boldsymbol{Q}\boldsymbol{u}_g\right)\cdot \boldsymbol{n} dS = 0 \quad (1)$$

where the term $\boldsymbol{f} = (\boldsymbol{F}+\boldsymbol{F}_v, \boldsymbol{G}+\boldsymbol{G}_v, \boldsymbol{H}+\boldsymbol{H}_v)$ represents the net flux across the cell surfaces; $\boldsymbol{u_g}$ is the velocity of the moving grid; others are defined as follows:

$$\boldsymbol{Q} = \begin{bmatrix} u \\ v \\ w \\ 0 \end{bmatrix},\ \boldsymbol{q} = \begin{bmatrix} u \\ v \\ w \\ p \end{bmatrix},\ \boldsymbol{F} = \begin{bmatrix} u^2 + p \\ uv \\ uw \\ \gamma u \end{bmatrix},\ \boldsymbol{G} = \begin{bmatrix} vu \\ v^2 + p \\ vw \\ \gamma v \end{bmatrix},$$

$$\boldsymbol{H} = \begin{bmatrix} wu \\ wv \\ v^2 + p \\ \gamma w \end{bmatrix},\quad \boldsymbol{F}_v = -\frac{1}{Re}\begin{bmatrix} 2u_x \\ u_y + v_x \\ u_z + w_x \\ 0 \end{bmatrix},$$

$$\boldsymbol{G}_v = -\frac{1}{Re}\begin{bmatrix} v_x + u_y \\ 2v_y \\ v_z + w_y \\ 0 \end{bmatrix},\ \boldsymbol{H}_v = -\frac{1}{Re}\begin{bmatrix} w_z + u_x \\ w_y + u_z \\ 2w_z \\ 0 \end{bmatrix}, \quad (2)$$

where, γ is the pseudo-compressibility coefficient; p is pressure; u, v, w are the x, y, z velocity components in the Cartesian coordinate system; t denotes physical time; τ is pseudo time; Re is Reynolds number. Note that the term $\boldsymbol{q}$ associated with pseudo time is designed for an inner-iteration at each physical time step, and will vanish when the divergence of velocity is driven to zero so as to satisfy the equation of continuity. Time-dependent solutions of the incompressible NS equations are formulated in an ALE (Arbitrary Lagrangian-Eulerian) manner with the FVM (Finite Volume Method) and are performed in a time-marching manner with a pseudo-compressibility method; we enforce conservation of mass and momentum in both time and space.

* Corresponding author: current affiliation is Department of Aeronautics and Astronautics, School of Engineering, Tokai University, 4-1-1 Kitakaname, Hiratsuka-shi, Kanagawa 259-1292, Japan, Email: inada@tokai-u.jp.
** Current affiliation is Mitsubishi Electric Company, Ltd.

A multi-blocked, overset grid method is incorporate into the CFD solver which uses two inner grids around the left and right wings and one large outer or background grid around the body, each of which is modeled to fit the object-specific structure (body or wing) as shown in Fig. 1 and moves in accordance with the motion of each object. The wing and body grids comprise 37x33x16 and 45x45x51 cells, respectively. The outer boundary of the body grid is approximately 30 mean chord length or about 5 times of span length of one wing from the body surface. A trilinear interpolation technique ensures the communication of velocities and pressures among overlapping grids.

B. Kinematics of flapping motion

The wingbeat is represented by the combination of three basic beating motions, flapping, lead-lag, and feathering, which denote the up- and downward motion of the wing within the stroke plane, for- and backward motion of the wing perpendicular to the stroke plane, and the rotation around the wing base-to-tip axis, respectively as shown in Fig. 2.

The kinematics of these three motions are described by using three angles, i.e. the positional angle (flapping angle) θ, the elevation angle (lead-lag angle) ϕ and the feathering angle α in terms of geometric angle of attack of a wing (AoA). These angles are expressed in the mathematical forms by using the Fourier series, such as:

$$\begin{aligned}\phi(t) &= \sum_{n=0}^{3}\left[\phi_{cn}\cos(2knt) + \phi_{sn}\sin(2knt)\right] \\ \theta(t) &= \sum_{n=0}^{3}\left[\theta_{cn}\cos(2knt) + \theta_{sn}\sin(2knt)\right] \\ \alpha(t) &= \sum_{n=0}^{3}\left[\alpha_{cn}\cos(2knt) + \alpha_{sn}\sin(2knt)\right]\end{aligned} \tag{3}$$

where t is a dimensionless time; k is reduced frequency; n is an integer varying from 0 to 3; and the coefficients $\phi_{cn,sn}$, $\theta_{cn,sn}$, $\alpha_{cn,sn}$ can be determined from the measured kinematic data. In this study, two types of wing motions are used, i.e. hovering and forward moving

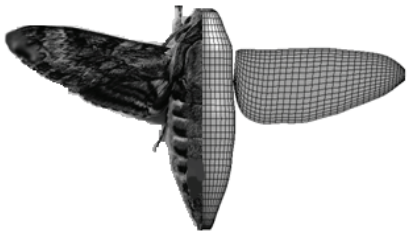

(a) Real and modeled morphologies of hawkmoth wing and body.

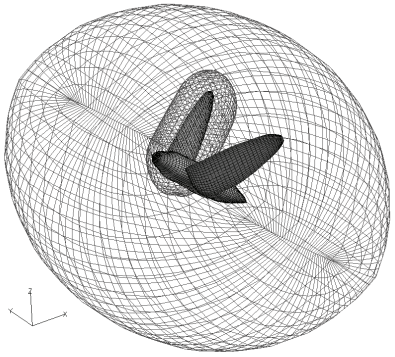

(b) Computational grid system (only right wing and body grids are drawn).

Fig. 1. Computational grid and wing-body morphologies

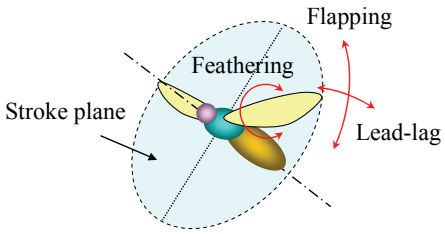

Fig. 2. Definition of angles

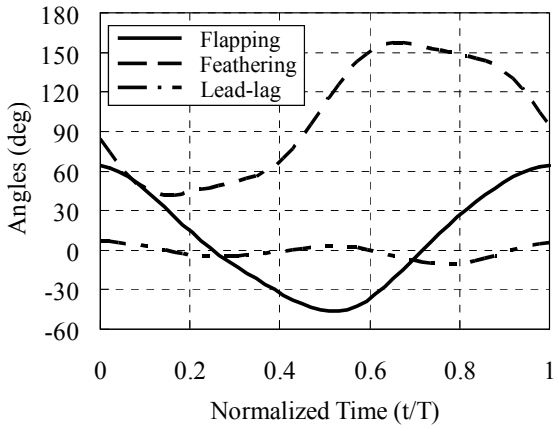

(a) Hovering flight (V=0m/s)

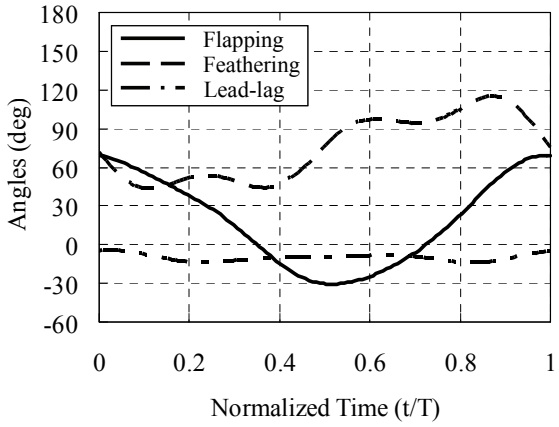

(b) Forward moving flight (V=2.9m/s)

Fig. 3. Time history of wing kinematics

flights. Time history of three angles for two motions is shown in Fig. 3. More details can be found in other literatures[2, 3].

C. Acoustic Analysis

The acoustic analysis is based on the Ffowks Williams and Hawkings (FW-H) equation[4,5], which is a solution of wave equation rearranged from compressible NS equation, and expressed as a following equation:

$$p(x,t) = \frac{1}{4\pi}\left(\frac{\partial}{\partial t}\int \frac{\rho_0 v_n}{r\Lambda} d\Sigma + \frac{1}{c_0}\frac{\partial}{\partial t}\int \frac{p_b \cos\theta}{r\Lambda} d\Sigma + \int \frac{p_b \cos\theta}{r^2\Lambda} d\Sigma\right) \quad (4)$$

where $p(x, t)$ is a sound pressure at a specified position x at time t; ρ_0, v_n, r, and c_0 denote the air density, the velocity component normal to the wing surface, the distance of the observer from the wing surface, and the sound speed, respectively; p_b, θ, and Σ denote the pressure distribution of wing surface, the angle between the direction normal to the wing surface and the observer point direction, and the influential surface, respectively. The symbol Λ is defined as

$$\Lambda \equiv (1 + M_n^2 - 2M_n \cos\theta)^{1/2} \quad (5)$$

where M_n denotes the Mach number of wing surface speed in the direction normal to the surface.

In Eq. 4, quadrupole sound source is neglected because the acoustic power of sound from quadrupole source is small and negligible under low Mach-number condition as in the flow around insect flapping wings. The pressure on the wing surface p_b is given from CFD results and other values are calculated from wing kinematics and morphology. More details can be found in the other literature[6].

III. RESULTS AND DISCUSSION

Calculations are conducted for two different flight modes of hawkmoth, i.e. hovering flight and forward moving flight. The body and motion parameters are shown in Table 1. The pressure distribution calculated by CFD is shown in Fig. 4, which is the pressure distribution on the wing upper surface moving in two flight modes. This is a momentary pressure distribution when the wing executes a downstroke and passes through the horizontal plane. Although a little difference exists, pressure distribution of both hovering (V=0m/s) and forward moving flights (V=2.9m/s) have distinct negative pressure near the wing leading edge, which is generated by the leading edge vortex (LEV). At this moment, the opposite side of the wing, i.e. lower side of the wing, has relatively strong positive pressure and thus generates a lift in collaboration with upper surface's negative pressure. This situation of pressure distribution on the upper and lower surfaces of the wing is reversed when the wing executes upstroke, resulting in the periodic pressure change during one flapping cycle on both surfaces of the wing. This periodic pressure change acts as the major source of flapping sound.

Table 1. Body and motion parameters used in the CFD and acoustic calculations.

Parameters	Hovering	Forward moving
Wing (one wing)		
Span length, R (mm)	48.5	52.1
Mean chord length, C_m (mm)	18.3	18.3
Moving speed, V (m/s)	0.0	2.9
Wing beat frequency, f (Hz)	26.1	26.1
Flapping cycle, T (sec)	0.0383	0.0383
Reynolds number, Re	6167	5623
Reduced frequency, k	0.2968	0.3256
Stroke plane angle (deg)	15.0	44.4
Body angle (deg)	39.8	19.9

Figure 5 shows the sound wave calculated by using FW-H equation (Eqs. 4 and 5) at three different observation points, i.e. fore, lateral, and downward points, each of which is 10 wing span length from the origin (= midpoint of two wing bases). Waves at front observation point (A in Fig. 5) show relatively simple

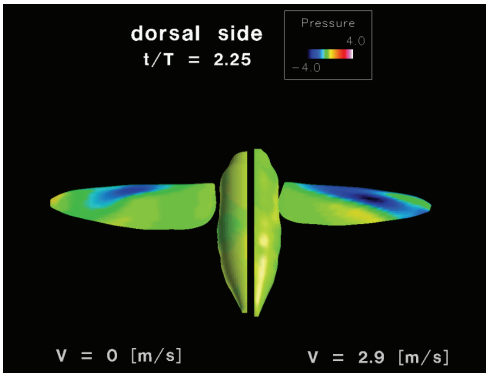

Fig. 4. Pressure distribution on the wing and body surface of hawkmoth in hovering (left) and forward moving flight (right) (Time in this figure is normalized by T/3).

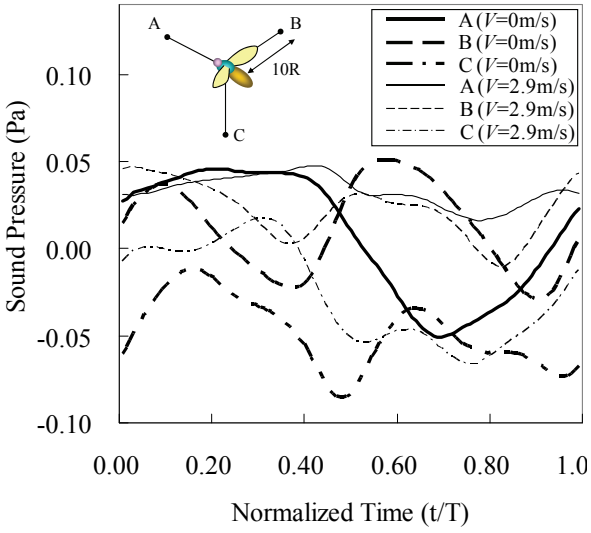

Fig. 5. Sound waves calculated at three different observation points.

variation for both hovering and forward moving flights, which have a tendency to fluctuate at the same frequency as the flapping motion of insect (=base frequency). Whereas, at the lateral and downward observation points (B and C in Fig. 5, respectively), waves distinctly have higher component of waves. This can be confirmed in Fig. 6 which shows the frequency component distribution of both flight modes at different observation points. The waves at front observation point (A in Fig. 5) show distinct peaks at the base frequency, i.e. flapping frequency, for both hovering (V=0m/s) and forward moving flight (V=2.9m/s), whereas the waves at lateral or downward observation points (B and C in Fig. 5, respectively) have distinct peaks at the second or higher harmonics except at the downward point of the forward moving flight.

The possible explanation for this result is illustrated in Fig. 7. As shown in Fig. 7(a), the wing approaches to the front observation point during downstroke with its positive pressure of air on the lower side of the wing orienting to the front observation point, and then the wing suppinates and retreats from this point during upstroke orienting its positive pressure of air on the upper surface of the wing to this point, resulting in the change of air pressure from positive to negative once during one flapping cycle and thus causing the dominance of base frequency of sound at the front observation point. In case of lateral observation point, interaction between the positive and negative pressure of air and the lateral observation point occurs twice during one flapping cycle as shown in Fig. 7(b), once in the downstroke and another once in the upstroke because the pair of positive and negative pressure of air around the wing passes by the this point in each stroke, thus resulting in the domination of second harmonics of sound at this point. This relationship between the position of observation point and the positive and negative pressure of air around the wing can be applicable to both hovering and forward moving flights because the flight speed (V=2.9m/s) is significantly small compared to the sound speed (≅ 340m/s), and thus the effect of flight speed on this positional relationship can be negligible, resulting in the similar frequency component for both hovering and forward moving flights as shown in Fig. 6. Doppler Effect should be considered in case the sound at the front and the backward observation points are compared for the forward moving flight. The dominance of the first or the second harmonics, however, may remain unchanged because the Doppler Effect only shifts the frequency peak to higher or lesser frequency for the front or the backward observation point, respectively. Consequently, it can be said that the component of the sound differs depending on the position of observation point, i.e. the base frequency dominates at the front observation point and may also dominate at the rear observation point, and the second or higher harmonicsis dominant at other observation points, especially at side, top, or bottom.

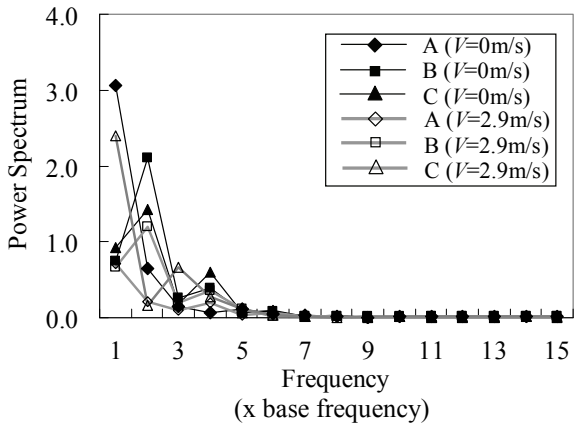

Fig. 6. Frequency component of flapping sound. A-C in the legends denotes the observation point shown in Fig.5.

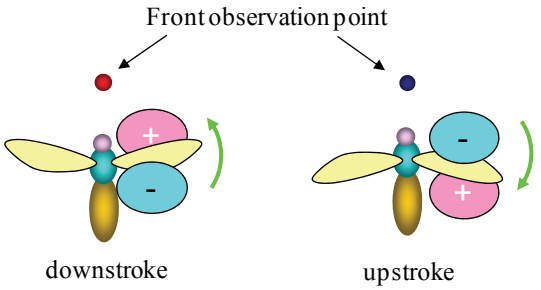

(a) Front observation point

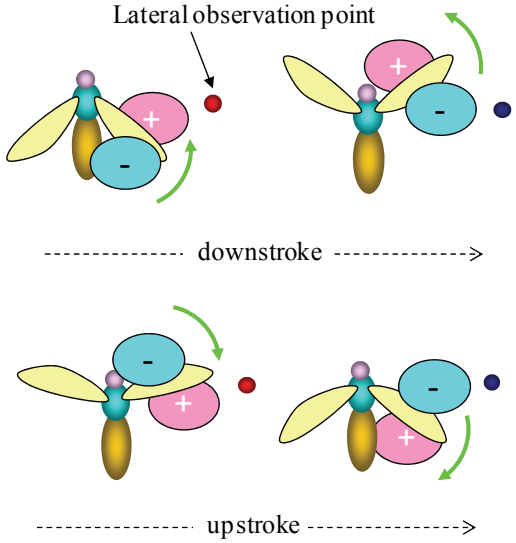

(b) Lateral observation point

Fig. 7. Schematics to show the positional relationship between observation point and wing.

Figure 8 shows the hemisphere display of average sound pressure level (SPL) during one flapping period. This figure can show the dependency of sound intensity on the direction where it transmits, i.e. the directivity of transmission in the flapping sound. It is clearly shown that the flapping sound has distinct directivity to transmit downward and backward, i.e. nearly perpendicularly to the flapping plane, as indicated by the maximum SPL position in Fig. 8. In the hawkmoth used in this study, the angle of flapping plane measured from the horizontal plane is larger in the forward moving flight than in the hovering flight as shown in Table 1, thus leading to the strong SPL at more backward direction in the forward moving flight than in the hovering flight. It also shows a weak transmission in the direction parallel to the flapping plane. In Fig. 8, this weakness of transmission is shown more clearly in the forward moving flight than in the hovering flight.

Consequently, the characteristics of flapping sound under two different flight modes are investigated and the results show the marked similarities in the frequency components of sound at several observation points. Although not distinct, the difference exists in the direction in which the sound transmits most strongly. These results can promote our understanding on the mechanism of sound generation and its control in the insect flight, and thus providing insights on the control method of man-made flapping flyers.

References

(1) Drosopoulos, S. and Claridge, M. F. ed, *Insect Sound and Communication, Physiology, Behavior, Ecology, and Evolution*, (2006), CRC press, Taylor and Francis Group, Florida, USA.

(2) Liu, H., and Kawachi, K., A Numerical Study of Insect Flight, *Journal of Computational Physics.*, Vol. 146(1998), pp.124-156.

(3) Aono, H., Liang, F., Liu, H., Near- and far-field aerodynamics in insect hovering flight: an integrated computational study, *Journal of Experimental Biology*, Vol. 211(2008), pp.239-257.

(4) Ffowcs Williams, J. E., Hawkings, D. L., Sound Generation by Turbulence and Surfaces in Arbitrary Motion, *Philosophical Transactions of the Royal Society of London*, A 264(1969), pp. 321-342.

(5) Farassat, F., Theory of Noise Generation from Moving Bodies with an Application to Helicopter Rotors, NASA TR R-451, Dec., (1975).

(6) Inada, Y., Aono, H., Liu, H., Aoyama, T., Numerical Analysis of Sound Generation of Insect Flapping Wings, *Theoretical and Applied Mechanics Japan.*, Vol. 57(2009), pp.437-447.

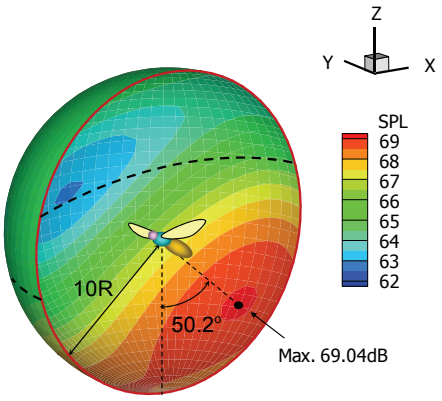

(a) Hovering flight (V=0m/s)

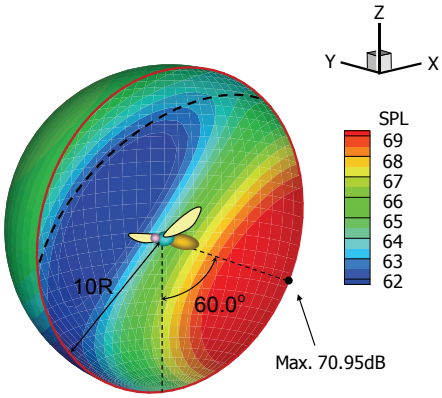

(b) Forward moving flight (V=2.9m/s)

Fig. 8. Hemisphere display of sound pressure level around the insect. The dotted line on the surface indicates the intersection of the stroke plane.